Visualization and back pressure analysis of water transport through gas diffusion layers of proton exchange membrane fuel cell

Tsung-Lin Liu [a], Chin Pan [a,b,c,*]

[a] Department of Engineering and System Science, National Tsing Hua University, Hsinchu 30013, Taiwan, ROC
[b] Institute of Nuclear Engineering and Science, National Tsing Hua University, Hsinchu 30013, Taiwan, ROC
[c] Low Carbon Energy Research Center, National Tsing Hua University, Hsinchu 30013, Taiwan, ROC

ARTICLE INFO

ABSTRACT

Transport of water through the gas diffusion layer (GDL) is explored to simulate the water flow in the cathode of a proton exchange membrane fuel cell (PEMFC). In this study, several commercial GDL media, including carbon paper and carbon cloth with or without a microporous layer (MPL), are employed. Liquid water is injected through the GDL media, and the differential pressure drop is measured to analyze the dynamic features of the water flow through the different structures of the GDL samples. Moreover, by combining the top-view images of the water droplet that emerges out of the GDL with the results of the dynamic measurement of the differential pressure drop, the water saturation inside the GDL after the water breakthrough through the GDL is analyzed. The "self-eruption transport" mechanism, which may control the water contained inside the GDL regardless of the water generation rate, is observed in the GDL whose one side is treated with MPL only. This suggests that a GDL with single-side MPL treatment may help effectively water management.

1. Introduction

In recent years, the proton exchange membrane fuel cell (PEMFC) has received a great deal of attention for automotive applications because of its high energy density at low temperatures and low or zero emissions [1]. However, the performance of a PEMFC may experience limited oxygen transport due to the accumulated water blocking the pores in the catalyst layer (CL), gas diffusion layer (GDL), and/or gas flow channels (GC). This phenomenon, known as "water flooding," is a critical obstacle to getting higher efficiency and power density for a PEMFC. In order to alleviate such a limitation and further optimize the fuel cell design, it is important to understand the two-phase transport in the cathode.

The GDL is an important component serving as the support structure for the membrane. One of its major functions is to maintain the balance between membrane hydration and water removal. Therefore, in-depth understanding of the water transport in the GDL may enable the development of optimal GDL materials and structures to mitigate water flooding and provide uniform transport of oxygen. In the literature, various computational models and diagnostic tools have been developed and studied. Pasaogullari and

Wang [2] studied the physics of water transport in both hydrophilic and hydrophobic GDLs and concluded that liquid water transport across the GDL is controlled by capillary forces. Furthermore, Pasaogullari and Wang [3] developed the multi-phase mixture (M^2) model to study the two-phase transport of water and reactants in GDL with a microporous layer (MPL). Sinha and Wang [4] developed a pore network model and revealed that liquid coverage at the GDL–channel interface results in pressure buildup inside the GDL and that the water droplets break out from preferential locations. Schulz et al. [5] developed a three-dimensional model to explore the water distribution in the gas diffusion medium and found that only a small number of pores are occupied by liquid water at breakthrough. Wang and Van Nguyen [6] suggested that capillary properties of the GDL have a more significant effect on the fuel cell performance than those of the CL. Moreover, a high capillary diffusion capability and low hydrophilic porosity results in better fuel cell performance.

Recently, many diagnosis techniques like neutron imaging [7–10], X-ray techniques [11–13], and optical photography [14–20] have been employed for in situ measurement of liquid water distributions in an operating fuel cell. However, because the fuel cell components are relatively thin and the water transport is rapid, such in situ measurements are of limited temporal or spatial resolutions [21]. Moreover, the GDL is commonly treated with a hydrophobic agent, and an MPL is added between the GDL and CL to enhance the water discharge ability [22]; this makes in situ quantitative measurement of water transport in GDLs more difficult.

* Corresponding author at: Department of Engineering and System Science, National Tsing Hua University, Hsinchu 30013, Taiwan, ROC.
Tel.: +886 35715131x34320; fax: +886 35720724.
E-mail address: cpan@ess.nthu.edu.tw (C. Pan).

Nomenclature

a	coefficient ($mL\,S^{-1}$)
b	decay constant (S^{-1})
D	water back diffusion from cathode to anode ($m^2\,s^{-1}$)
d	thickness of GDL (m)
F	Faraday's constant ($C\,mol^{-1}$)
I	current density ($A\,m^{-2}$)
$j_{H_2O,cathode}$	water flux in cathode ($kg\,m^{-2}\,s^{-1}$)
K_m	permeability of membrane (m^2)
M_{H_2O}	molecular weight of water ($kg\,K^{-1}\,mole^{-1}$)
$\dot{Q}$	water flow rate ($m^3\,s^{-1}$)
$R(t)$	radius of droplet at time t (m)
$R_{d,i}$	droplet radius measured by CCD images (m)
$R_{d,th}$	droplet radius predicted from differential pressure data (m)
r_c	pore radius (m)
s_w	liquid saturation
t_0	initial time of water contact of the bottom of GDL (s)
t_b	time of liquid water breakthrough (s)
V	accumulated water volume (m^3)
V_{d2}	liquid discharge volume at t_2 (m^3)
V_p	GDL pore volume (m^3)
V_w	volume of water inside the GDL sample (m^3)
ΔC_{c-a}	concentration gradient ($mol\,m^{-3}$)
ΔP	differential pressure across the GDL (kPa)
ΔP_c	critical capillary pressure (kPa)
ΔP_{c-a}	differential pressure of cathode to anode (kPa)
δ	thickness of membrane (m)
ε	porosity
λ_{drag}	electro-osmotic drag coefficient
μ_l	water viscosity ($m^2\,s^{-1}$)
θ	contact angle ($^\circ$)
ρ_l	water density ($kg\,m^{-3}$)
σ	surface tension of water ($N\,m^{-1}$)

Therefore, in order to deepen the understanding of the liquid water transport mechanism and distribution in GDL, many techniques for ex situ measurements has been developed and employed.

Nam and Kaviany [23] used an environmental scanning electron microscope to observe the vapor condensation in GDL and proposed a "tree-like" transport mechanism. Lister et al. [24] and Bazylak et al. [25] used fluorescence microscopy to capture images of the liquid water transport through the GDL. They revealed that the transport is dominated by "fingering and channeling." Furthermore, Bazylak et al. [26] employed a simplified experimental model of the system to investigate the stability of the droplet on plates of different wetting properties and the potential for liquid entrapment in the GDL/land contact area. They suggested that the hydrophobic land areas are preferable for mitigating the accumulation of liquid water. Gao et al. [27] employed a confocal microscope to visualize liquid water flow through a GDL. They found an unstable "column flow" in GDLs, and the results agreed with those proposed by Litster et al. [24]. Medici and Allen [28] established a capillary and viscosity phase diagram to explore the water transport characteristics and found that the GDL morphology has a significant effect on the fluid displacement. Benziger et al. [29] and Kimball et al. [30] developed a pressurized water filtration system to diagnose the liquid water transport through GDLs. They proposed that the best GDL material will have bimodal pore distribution, large pores to carry water from the membrane/electrode interface to gas flow channel, and small pores to carry oxygen from the gas flow channel to membrane/electrode interface.

To understand the interaction of liquid water with the GDL material, the critical relationships of capillary pressure (P_c) versus liquid water saturation (S_w) were studied by some groups, e.g., Gostick et al. [31–33] and Fairweather et al. [34,35]. The effects of wettability and MPL were also explored in these studies. Recently, Chou et al. [36] studied the influence of hydrophobic treatment on the GDL and found that water drainage is controlled by the pore configuration instead of the hydrophobicity. Lu et al. [37] compared the water breakthrough dynamics of GDL samples with or without an MPL.

The results in the literature suggested that the MPL not only limits the number of water entry locations into the GDL but also stabilizes the water paths. Overall, the interplay of the liquid water movement and GDL pore structure has been extensively investigated.

This study investigated the transport phenomena of liquid water through GDLs with four different morphologies to explore the water capillary flow mechanism inside the fuel cell. For this purpose, images of water breakthrough GDLs were recorded, and the differential pressure required to push water through different GDL samples were also measured simultaneously and analyzed theoretically. The patterns of breakthrough droplets, discharge ability of GDLs, and water saturation for GDLs were quantified.

2. Experimental details

2.1. Experimental setup

Fig. 1(a) shows the experimental setup, which consists of a syringe pump (KD Scientific 200 series), test module, charge-coupled device (CCD) system, and related control and measurement systems. For the test module (Fig. 1(b)), a piece of GDL was mounted between two polycarbonate (PC) material plates with six screws on the base plate. Both the bottom PC plate and stainless steel tube are opened with a window of 20 mm × 5 mm for the fluid to transport through. The upper PC plate is equipped with a 24 mm × 11 mm window open to atmosphere for flow visualization. The front-end of the stainless steel tube is connected with a syringe pump which drives the water flow, and the back-end is connected with a differential pressure transmitter, which measures the pressure difference between the back pressure and atmospheric pressure. Thus, water flows from the front-end to the open window. The differential pressure transmitter (HUBA 692) with an operating range of 0–10 kPa, precision of 0.5% over the entire range, and connected to the data recorder (Yokogawa MX100) was used to measure the differential pressure relative to the atmosphere pressure. Videos of flow visualization were recorded by a CCD camera with a zoom lens, and its digital resolution was 640 × 480 pixels. A timer was set on the upper left corner of the videos to synchronize the image with the differential pressure data.

2.2. Gas diffusion layers

Flow through four GDLs with different morphologies i.e., carbon paper, carbon cloth, carbon cloth with single-sided MPL, and carbon cloth with double-sided MPL was studied. Fig. 2 shows the SEM images of the above four GDLs. The brand, thickness, porosity, surface and bulk density of these four GDLs are listed in Table 1. Notably, carbon cloth and paper had the same thickness of 350 μm and porosity of 78%. Carbon cloth with single- and double-sided MPLs are thicker and of lower porosity than cloth and paper (73–75%). All the GDL media are commercially available, and cut to the dimensions of 30 mm × 15 mm for used in the experiment.
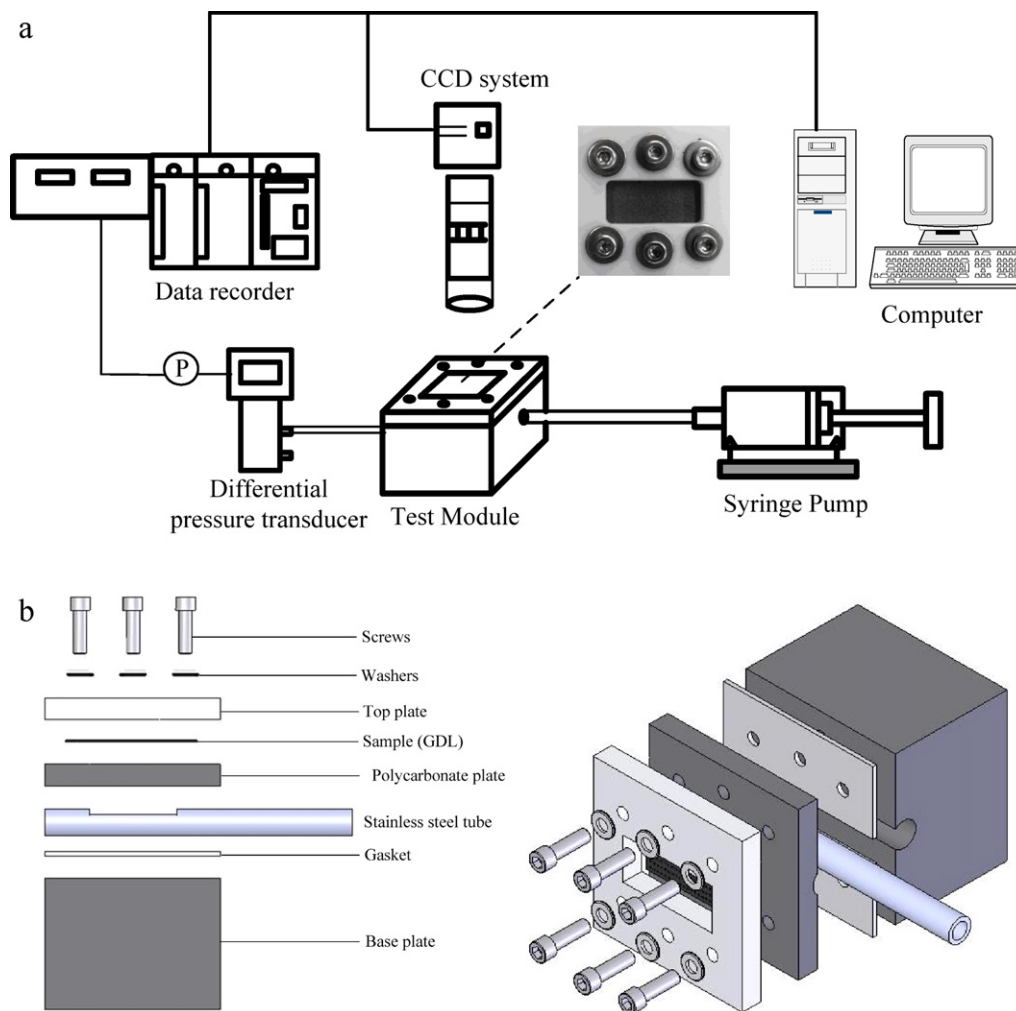
Fig. 1. Experiment apparatus: (a) overall system setup (b) side and isometric views of the test module.

2.3. Experimental procedure

Each GDL sample was dried in an oven at 80 °C for 30 min before each experiment, and then the dried GDL sample was sandwiched between top and down plate with six screws tightened to 2 Nm. The water flow rates of syringe pump were set to 0.01, 0.02, and 0.05 (mL min^{-1}) to simulate the water generation in an actual PEMFC, as will be discussed in the next section. The fluid was injected into the stainless tube, and then permeated into the GDL from the bottom side of the GDL by a syringe pump. (For single-sided MPL, the MPL-treated side is the bottom side.) The differential pressure between the back pressure and atmospheric pressure was recorded simultaneously with flow visualization of droplet formation on the top surface of the GDL by a CCD camera during water transport through

the GDL process. All the experiments were carried out in a lab with air conditioning all the time, so the room temperature was around 24–26 °C and the relative humidity was around 50–60%.

2.4. Water flow rate for syringe pump

In this study, the water flow rate was chosen to simulate the water generation rate in the cathode of a PEMFC. The water flux arrival and production at the cathode can be expressed as [38]

$$j_{H_2O,\text{cathode}} = -D\frac{\Delta C_{c-a}}{\delta} + \frac{I}{F}\lambda_{\text{drag}} + \frac{I}{2F} - \frac{K_m}{\mu_l}\Delta P_{c-a}\frac{\rho_l}{M_{H_2O}} \qquad (1)$$

The four terms on the right side account for the four different modes of water transport and generation: back diffusion driven

Table 1
Brand and properties of GDL samples of the present study.[a]

Material	Carbon cloth	Carbon paper	LT1200W	HT2500W
Type	Cloth	Paper	Cloth/single-sided MPL	Cloth/double-sided MPL
Brand	B-1 designation A[c]	TGP120[b]	LT1200W[c]	HT2500W[c]
Thickness (μm)	350	350	370	450
Porosity (%)	78	78	73[d]	75[d]
Surface density (g cm^{-2})	12.8[d]	8.6[d]	14.5[d]	28.3[d]
Bulk density (g cm^{-3})	0.37[d]	0.45	0.47[d]	0.63[d]

[a] Given by manufacturer except where noted.
[b] Toray Corp., Tokyo, Japan.
[c] E-TEK Inc., Somerset, NJ, USA.
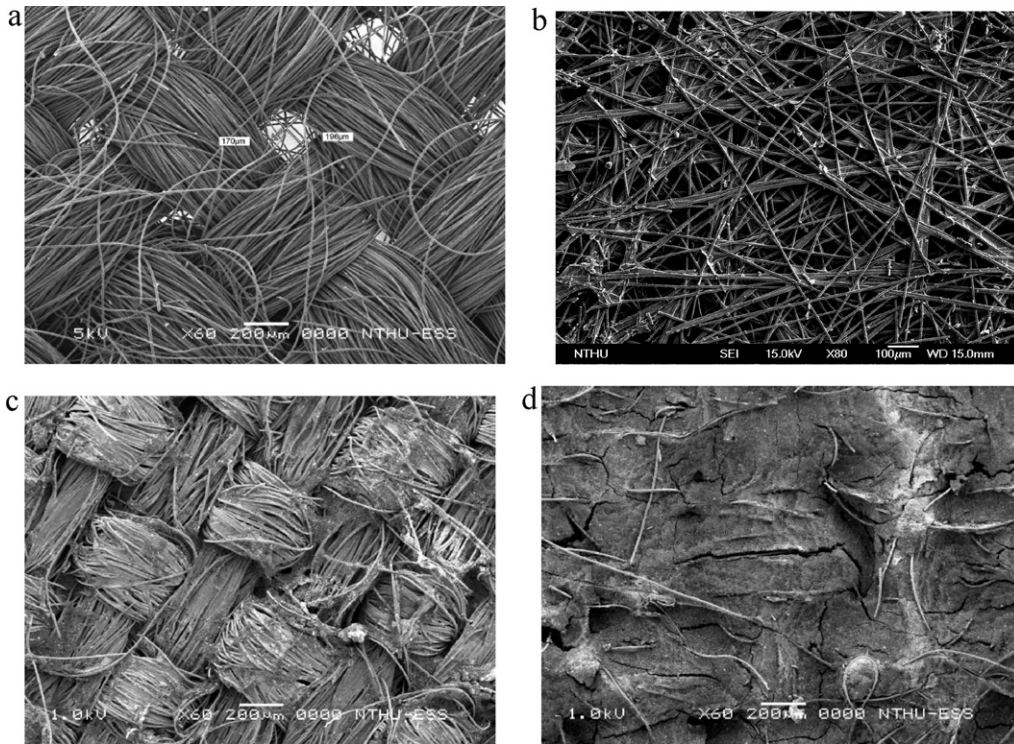[d] Measured using a capillary flow porometry at ITRI (CFP-1200-A, PMI).

Fig. 2. SEM image of (a) carbon cloth (B-1 designation A), (b) carbon paper (TGP-120), (c) carbon cloth/MPL (LT1200W) and (d) carbon cloth/MPL-D (HT2500W).

by the concentration gradient; electron-osmotic drag, which is proportional to the current density; water generation rate in the cathode; and permeation driven by the hydraulic pressure difference between the anode and cathode, respectively. The back diffusion and permeation terms are usually comparatively small and thus were neglected for simplicity. Consequently, the total flux of water in the cathode can be expressed as

$$j_{H_2O,cathode} = \left(\lambda_{drag} + \frac{1}{2}\right)\frac{I}{F} \qquad (2)$$

where the electro-osmotic drag coefficient (λ_{drag}) is about 2 (H_2O/H^+) for a Nafion® 117 membrane at room temperature when fully hydrated [39]. The three water flow rates employed in the experiment (0.01, 0.02, and 0.05 mL min^{-1}) correspond to current

densities of 0.36, 0.72, and 1.8 A cm^{-2} in a real PEMFC based on Eq. (2).

3. Results and discussion

3.1. Liquid water breakthrough in GDL samples without MPL

To investigate the effect of the water flow rate on the transport behavior through different kinds of GDLs, breakthrough images were recorded and the differential pressure across the GDL was measured synchronously. Fig. 3 illustrates the dynamic images of an emerging water droplet from the carbon paper for a water flow rate of 0.01 mL min^{-1}. The droplet grows approximately as a sphere because the GDL surface is hydrophobic; in our laboratory, the
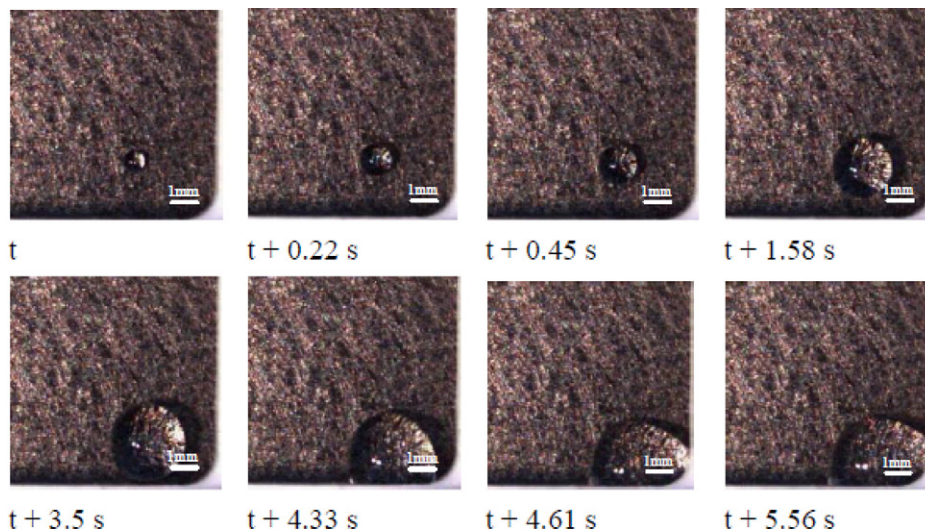

Fig. 3. Dynamics of water droplet at a flow rate of 0.01 mL min^{-1} after the breakthrough of carbon paper.
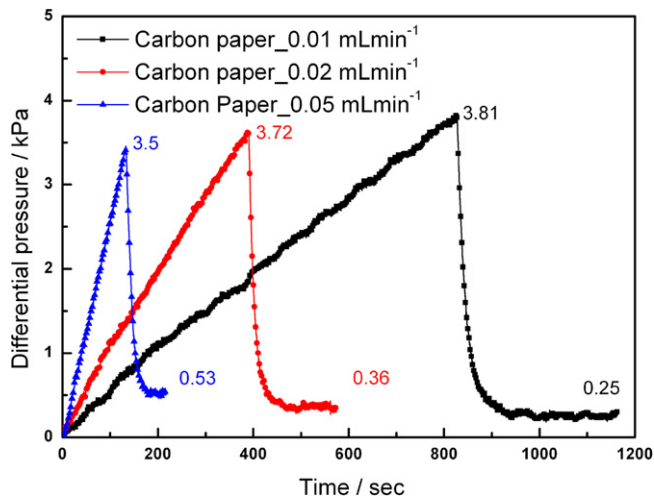
Fig. 4. Differential pressure profile of carbon paper with flow rates of 0.01 mL min^{-1} (black), 0.02 mL min^{-1} (red), and 0.05 mL min^{-1} (blue). (For interpretation of the references to color in this figure legend, the reader is referred to the web version of the article.)

Fig. 5. Differential pressure profile of carbon cloth with syringe pump flow rates of 0.01 mL min^{-1} (black), 0.02 mL min^{-1} (red), and 0.05 mL min^{-1} (blue). (For interpretation of the references to color in this figure legend, the reader is referred to the web version of the article.)

contact angle was measured as 122°. A single water breakthrough spot appeared for several repeated trials. This suggests that there are few pores available for the transport of liquid water through the carbon paper.

Fig. 4 shows the corresponding differential pressure profiles for water flow through the carbon paper with injected flow rates of 0.01, 0.02, and 0.05 mL min^{-1}. The figure demonstrates that the back pressure continues to increase linearly until it reaches a peak value, at which the droplet breaks through and begins to appear on the GDL upper surface. The peak value is defined as the breakthrough pressure. Subsequently, the differential pressure sharply drops to a much lower and nearly steady value. If the flow rate is increased, a similar pattern for the pressure rise and drop appears. However, the slope of the pressure rise increases with the increase in flow rate. The pressure rise rate can be associated with water accumulated in the diffusion layer, while the steady pressure after the sharp drop may be related to the steady water contained in the medium. Therefore, the slope of the pressure rise and the steady pressure increase with increasing flow rate.

For the carbon cloth, the pressure rise and fall pattern is somewhat different (see Fig. 5). The differential pressure increases at a smaller rate at the beginning and at a larger rate after the pressure is greater than about 0.2 kPa. This occurrence is due to the higher flexibility of the carbon cloth. Moreover, the breakthrough pressure is about 1.1 kPa, which is much smaller than that for carbon paper (3.6 kPa). This suggests that the pore size for the carbon cloth is much larger than that for the carbon paper. The critical capillary pressure can be calculated from the Young–Laplace equation as

$$\Delta P_c = \frac{2\sigma \, \cos \theta}{r_c} \tag{3}$$

where σ is the surface tension of water (= 0.072 N m^{-1}), ΔP_c is the critical capillary pressure which is the average breakthrough pressure of each GDL sample, θ is the contact angle of water with the pore surface, and r_c is the pore radius. The pore diameter for the carbon paper and carbon cloth were calculated by Eq. (3) to be 42 and 130 μm, respectively; these values agree with the findings by Benziger et al. [29].

Notably, the differential pressure profile for the flow rate of 0.01 mL min^{-1} demonstrated a down-and-up pattern at 610 s. Such a peculiar pressure drop pattern reflects the fact that the water droplets emerge and grow. The second rise is caused by breaking of the liquid water passageway. The water delivering process
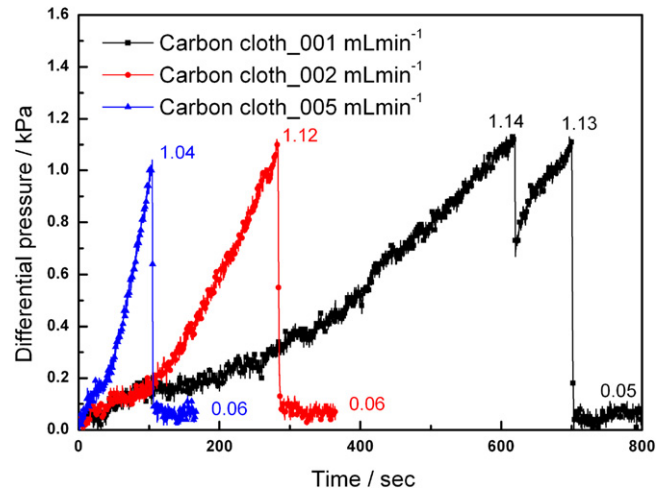
is discontinuous. After water re-accumulated for about 95 s, the breakthrough pressure was reached and the droplet emerged again at the same spot. The selected images shown in Fig. 6 demonstrate this interesting phenomenon.

Lu et al. [37] and Bazylak et al. [25] observed that the GDL without an MPL changed the breakthrough locations with time, but in this study, the carbon cloth was the only one for which this was observed, and it occurred rarely. The surface tension and carbon fibers' Teflon treatment may have led to the difference. The location changed only after the dismissed water droplet grew to achieve contact the sidewall of the upper window (Fig. 6) in this study. The water contact angle of the sidewall (material is polycarbonate) was much smaller than that of the GDL fibers, so when the droplet makes contact with the wall, it may be pull out of the GDL by surface force. Lu et al. [37] set a hydrophilic medium on top of the GDL to observe the breakthrough locations, so once the droplet breakthrough is sucked by the hydrophilic media, this can result in the "choke-off" effect. Moreover, the GDL without MPL employed by Lu et al. had Teflon treatment, but the one in this study did not.

3.2. Liquid water breakthrough for the GDL samples with MPL

Intermittent water breakthrough constantly appears in the GDL with the single-sided MPL. Fig. 7 demonstrates a cyclic differential pressure pattern when water transports through the GDL with single-sided MPL. After the first breakthrough pressure drop, the differential pressure displays cyclic values between about 2.45 and 2.7 kPa roughly every 20 s. The sawtooth-like pressure curve suggests that the water droplets emerge discontinuously. This implies that the GDL with the single-sided MPL can dismiss the liquid water inside its structure spontaneously. Corresponding to the differential pressure curve for a water flow rate of 0.01 mL min^{-1}, Fig. 8 illustrates the dynamic image of water droplets demonstrating a cyclic nature. The small droplets are discharged quickly and burst discretely at the same spot. The cyclic oscillation is characterized by explosive droplets that depart and remove water from the pores inside the GDL rapidly; this leads to insufficient supply of water, and some parts of the pores may become empty. The pores are refilled again after the supplied water accumulates to a sufficient back pressure. Such a peculiar water transport mechanism is called eruptive transport in the literature. Manke et al. [11] and Hartnig et al. [13], who employed the SGL 10 BB as gas diffusion
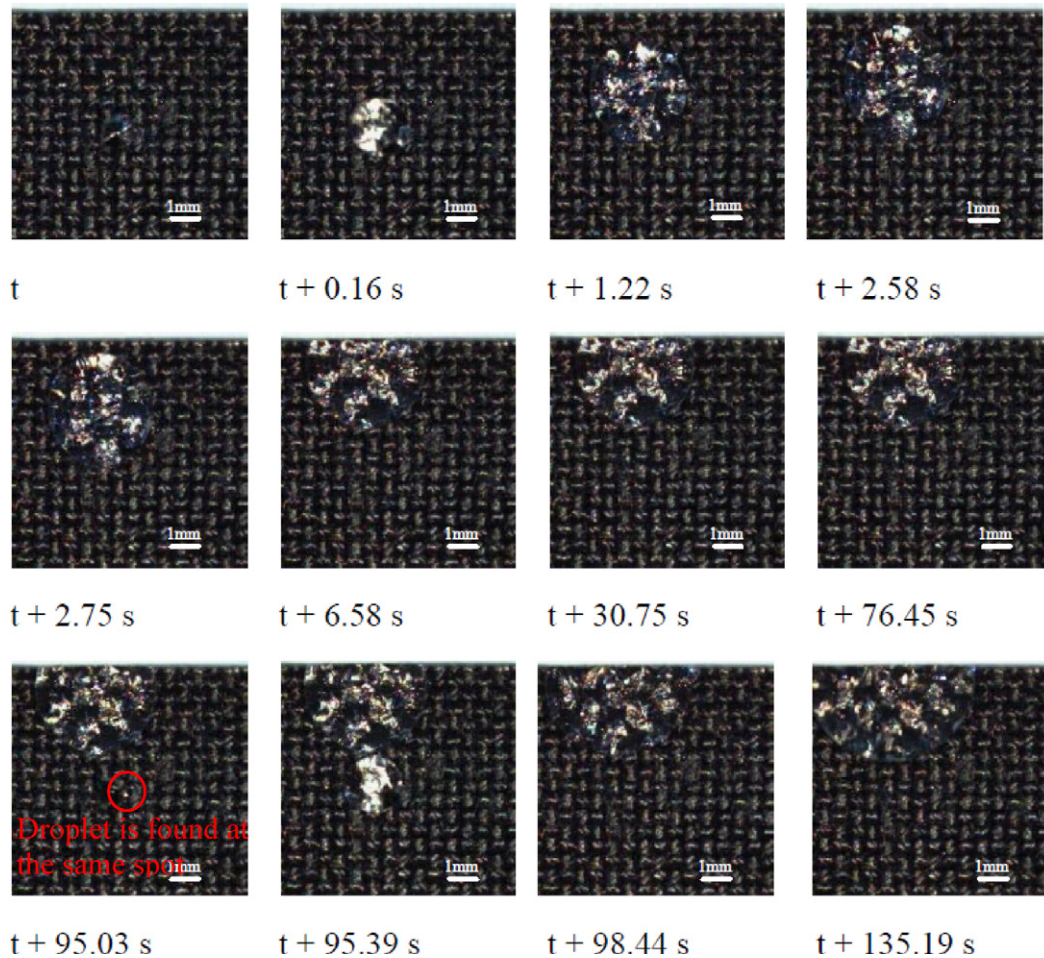
Fig. 6. Dynamics of water droplet at a flow rate of 0.01 mL min^{-1} after breakthrough of the carbon cloth and reemergence at the same spot until accumulation of enough pressure.

layer with single-sided MPL, reported a similar eruptive water transport.

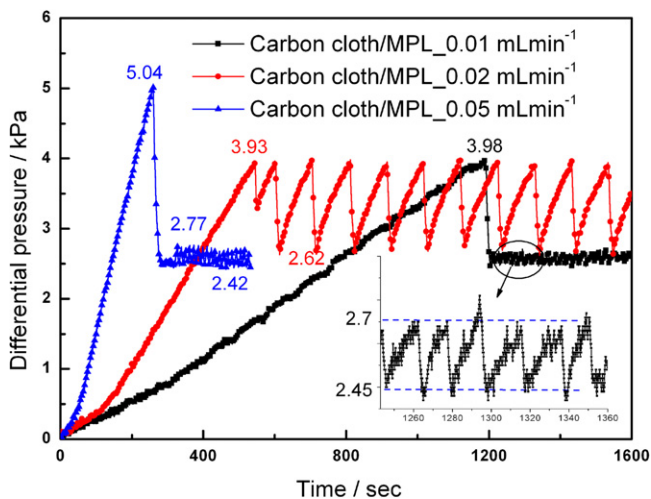Fig. 9 shows the differential pressure profile of the carbon cloth with double-sided MPL. The breakthrough pressures were higher than those for the other types of GDL used in this study. Such double-sided MPLs clearly increase the resistance of water flowing through the GDL.

It should be noted that the present study imposed a uniform boundary condition in front of the GDL layer, which is different from that in an actual PEMFC, the water produced from catalyst to GDL layer is a uniform water flux [40]. Consequently, the multi-droplets reveals from GDL in an actual PEMFC [16,17] were not observed in this study.

3.3. Differential pressure characteristics of different GDL samples

Table 2 summarizes some characteristics of differential pressure for three water flow rates through various kinds of GDL. In the linearly increasing pre-breakthrough period, different slopes of the pressure rise demonstrate different degrees of flexibility of the GDL. This indicates that the carbon cloth is flexible, while the carbon paper is more difficult to bend. Adding single- or double-sides of MPL also increases the hardness. However, both single-sided and double-sided MPL resulted in nearly the same slope. The effect of flexibility on the slope of the pressure rise in the pre-breakthrough period is a characteristic of the apparatus of this study and may be of less concern in an actual PEMFC in which the GDL is sandwiched between catalyst layer and bi-polar plate. The breakthrough pressure refers to the back pressure required to initially penetrate through the GDL, while the steady pressure refers to the liquid water that continually transports through the
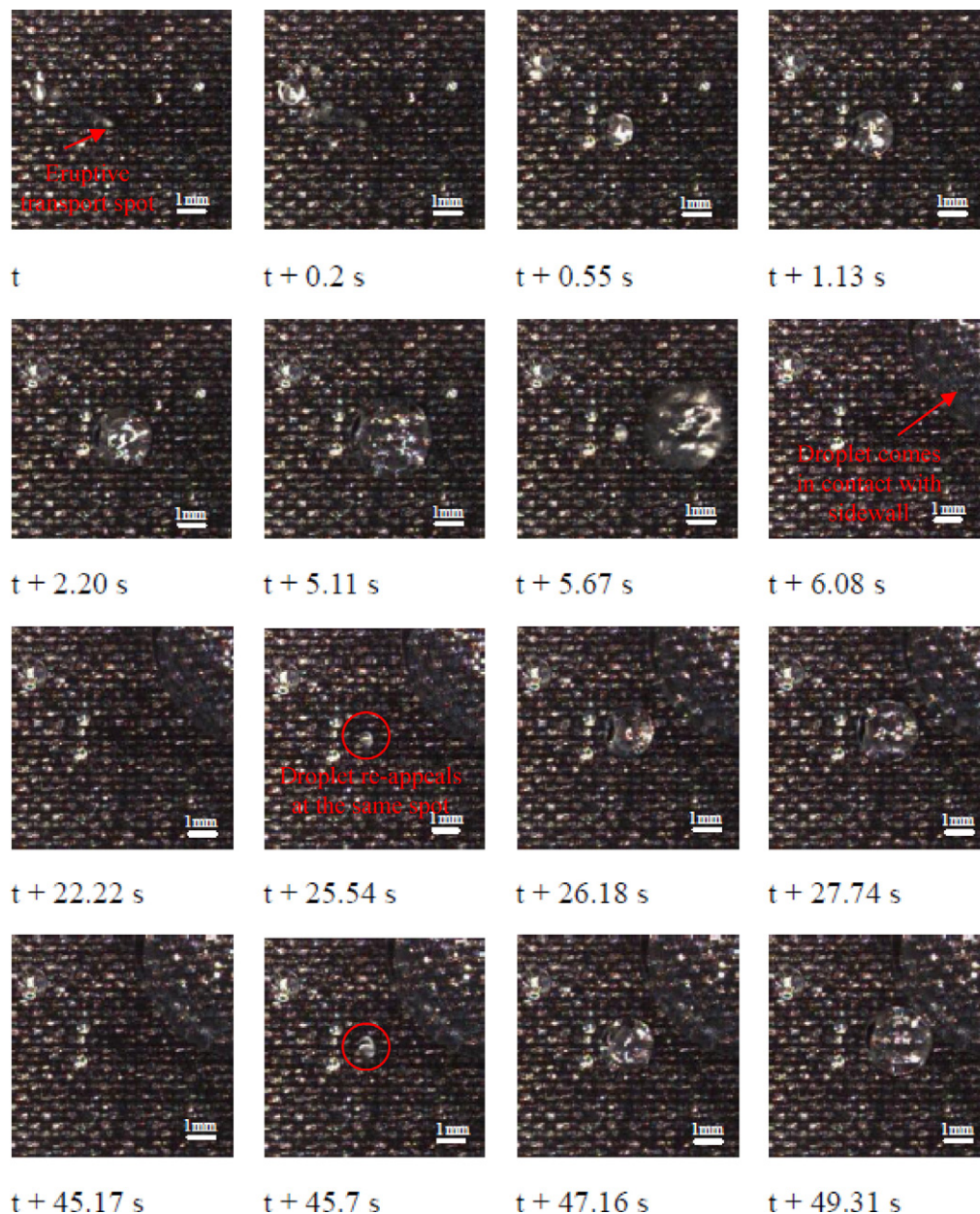

Fig. 7. Differential pressure profile of carbon cloth/MPL (LT1200W) with flow rates of 0.01 mL min^{-1} (black), 0.02 mL min^{-1} (red), and 0.05 mL min^{-1} (blue). (For interpretation of the references to color in this figure legend, the reader is referred to the web version of the article.)

Fig. 8. Dynamic images of water droplet at a flow rate of 0.01 mL min^{-1} after breakthrough of LT1200W.

GDL media at a steady state. For all types of GDL, the breakthrough pressure was always higher than the steady pressure; this suggests that the pressure to overcome the surface energy is much higher than that to drive the flow. This implies that once water transports through the GDL, the water can be easily carried out of the electrolyte/electrode interface, as suggested by Benziger et al.

[29]. Moreover, Table 2 demonstrates that for each kind of GDL, the breakthrough pressure is generally independent of the flow rate. The carbon cloth presents the lowest breakthrough pressure due to its large pores, while the carbon cloth with double-sided MPL has the highest pressure due to the relatively fine pores of both sides.

Table 2
Some measured differential pressure characteristics of GDL samples.

GDL	Carbon paper			Carbon cloth			a			b		
Flow rate[c]	(1)	(2)	(5)	(1)	(2)	(5)	(1)	(2)	(5)	(1)	(2)	(5)
Slope of pressure rise (Pa s^{-1})	4.62	9.79	26.9	1.84	3.97	10.1	3.34	7.21	19.38	3.06	7.3	20.2
Breakthrough pressure (kPa)	3.8	3.7	3.5	1.15	1.1	1.05	3.98	3.93	5.04	8.53	7.92	9.49
Steady pressure (kPa)	0.25	0.36	0.53	0.04	0.03	0.06	2.45[d]	2.56[d]	2.43[d]	1.26	2.95	6.33

a – carbon cloth with single-sided MPL.
b – carbon cloth with double-sided MPL.
  [c] Value in the parentheses is the ratio corresponding to the flow rate of 0.01 mL min^{-1}.
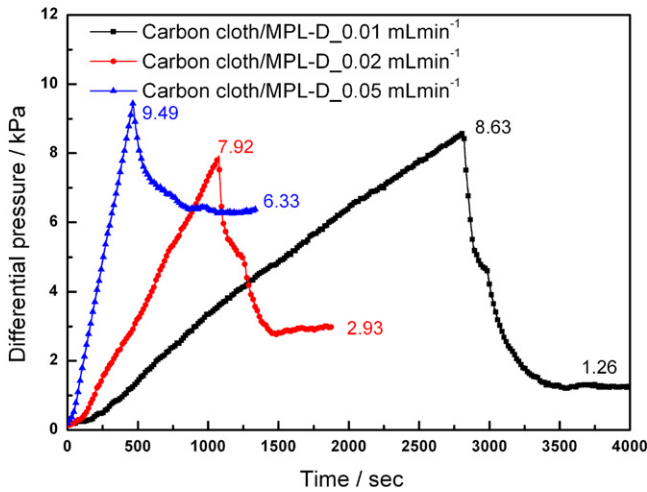 [d] The minimum differential pressure.

Fig. 9. Differential pressure profile of carbon cloth/two side MPL (HT2500W) with flow rates of 0.01 mL min^{-1} (black), 0.02 mL min^{-1} (red), and 0.05 mL min^{-1} (blue). (For interpretation of the references to color in this figure legend, the reader is referred to the web version of the article.)

Fig. 10. Schematic diagram of the hypothetical differential pressure during the liquid water breakthrough experiment.

For carbon paper and carbon cloth with double-sided MPL, the steady pressure rises with the increase in flow rate as Darcy's law suggests. However, for carbon cloth, which pores is relatively large the steady pressure drop is nearly vanishing, due to the limitation of the pressure transducer employed in this study. For carbon cloth with single-sided MPL, cyclic pressure drop appears and the minimum pressure drop is around 2.4–2.6 kPa (see Fig. 7) for all three water flow rate. This may be due to the vastly different microstructural and wetting characteristics resulting in water saturation discontinuity at the interface of GDL and MPL [3,23]. Accordingly, the carbon cloth with single-sided MPL might have the ability of self-controlling water saturation regardless of the water generation in the catalyst layer.

3.4. Liquid discharge rate

The differential pressure profile may reflect some important dynamic features of liquid water transporting through GDLs, such as flow characteristics, the water discharge ability, and liquid water saturation. Fig. 10 shows a typical differential pressure curve versus time during the process of liquid water through GDL experiment. The liquid pressure increases linearly as the continuously injected water accumulates inside the GDL during the time interval t_0 to t_b. Because there is no water coming out of the GDL, the linear increase in the differential pressure suggests that it is proportional to the accumulated water volume. Thus,

$$V = \dot{Q}t \quad (t \le t_b) \tag{4}$$

and

$$V \propto \Delta P \tag{5}$$

where V is the accumulated water volume, $\dot{Q}$ is the liquid water flow rate, and ΔP is the differential pressure across the GDL. After the time of liquid droplet breakthrough (t_b), the differential pressure begins to fall and eventually reaches a steady value. According to Fig. 10, if the water accumulates to time t_2 without breakthrough, the water volume is V_2. However, in a real process with the water drop breakthrough, the differential pressure at time t_2 drops to P'_2, which is equal to P_1 and corresponds to an the accumulated water volume of $V'_2 = V_1 = \dot{Q}t_1$. Thus, the total liquid discharge volume at t_2 can be expressed as:

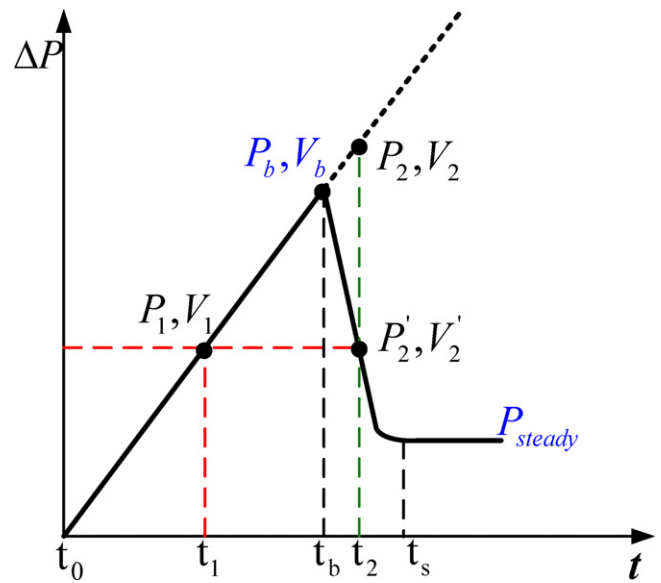$$V_{d2} = V_2 - V'_2 = V_2 - V_1 = \dot{Q}(t_2 - t_1) \tag{6}$$

The total liquid volume at any other time after liquid drop breakthrough can be determined similarly, and the discharge flow rate can be evaluated from its time derivative. The water discharge flow rate reflects the ability of GDLs to dismiss the water inside by itself. A large discharge flow rate suggests a better water transport ability. To be noted that, the GDLs employed in the present study may not be ideally elastic and the pressure change may have some degree of hysteresis, which is not considered in the analysis above.

Exploring the water discharge flow rate for different GDL samples is of great interest for water management in a real fuel cell. Fig. 11(a) and (b) shows the comparison of discharge flows for the GDL samples without and with MPL, respectively, at a water flow rate of 0.02 mL min^{-1}, which corresponds to a current density of about 0.7 A cm^{-2} in a real PEMFC. The figure clearly demonstrates that the GDL samples of carbon paper, carbon cloth, and carbon cloth with double-sided MPL (carbon cloth MPL-D) dismiss water continuously, and the drainage flow rates drop sharply from the high value to a nearly steady flow rate (0.02 mL min^{-1}). The discharge flow rate versus time for these three GDL samples may fit well to an exponentially decaying curve, as shown by the dash lines. However, the carbon cloth with single-sided MPL (carbon cloth/MPL) dismisses water with cyclic flow. The MPL added on one side of a GDL can changes the continuous water drainage transport mode to one with eruptive transport, which is a more effective mechanism for water removal.

To present the comparison more clearly, Fig. 12 illustrates the fitted curves of the GDLs with the continuous discharge flow rate shown in Fig. 11. These fitted curves may be expressed by the following general equation:

$$\dot{Q} = 0.02 + ae^{-bt} \tag{7}$$

where $\dot{Q}$ is the liquid discharge flow rate (mL min^{-1}), t is the time after liquid drop breakthrough measured in seconds, and the constant 0.02 accounts for the constant water flow rate being supplied. The coefficient a and decay constant b are 0.59 and 0.0893, respectively, for carbon paper; 3.02 and 1.25, respectively for carbon cloth; and 0.17 and 0.0231, respectively, for carbon cloth with double-sided MPL. The highest water discharge flow rate is at $t = 0$. The carbon cloth demonstrated the highest water discharge flow rate of 3.04 mL min^{-1}; this was followed by carbon paper at 0.61 mL min^{-1}, and the carbon cloth with double-sided MPL
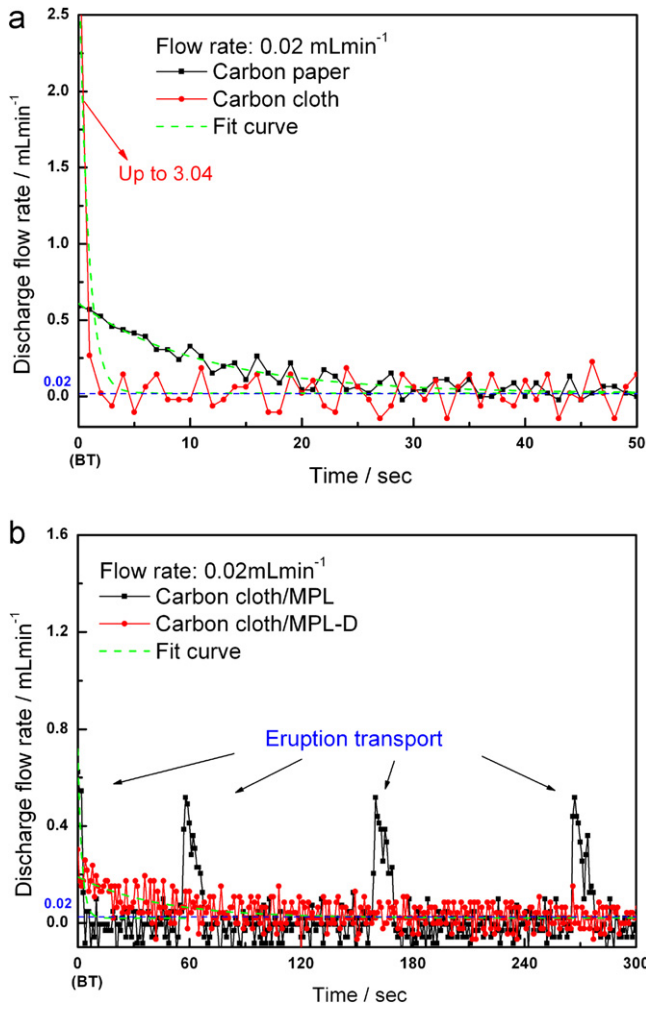
Fig. 13. Droplet radius growing curve of GDLs after the breakthrough time.

carbon paper, and 270 s for carbon cloth with double-sided MPL. In terms of water drainage ability, carbon cloth with single-sided MPL is the best candidate as the eruptive transport can empty the pores intermittently and effectively. Carbon cloth presented the second-highest liquid discharge flow rate, followed by carbon paper and then carbon cloth with double-sided MPL.

3.5. Liquid water saturation inside the GDL samples

The liquid saturation distribution in the GDL is also of significant interest as it is a key parameter indicating flooding occurrence in a fuel cell. It is reasonable to assume that the liquid droplet comes out of the GDL with a spherical shape. Thus, the discharge liquid flow rate can also be expressed as

$$\dot{Q} = \frac{d}{dt}\left(\frac{4\pi R(t)^3}{3}\right) \tag{8}$$

Substituting Eq. (7) to Eq. (8) and then integrating the resulting equation gives the droplet radius as a function of time for the three GDLs with continuous discharge:

$$R(t) = \left\{\frac{3}{4\pi}[0.02t + c(1 - e^{(-bt)})]\right\}^{1/3} \tag{9}$$

where c is 6.6, 2.42, and 7.34 for carbon paper, carbon cloth, and carbon cloth with double-sided MPL, respectively. Fig. 13 shows the comparison of the droplet radii visualized by CCD images and as given by Eq. (9) after breakthrough. In the figure, the breakthrough time, which is also considered as the time for the differential pressure begins to decay, is set to zero. The symbolic lines illustrate the radius measured based on CCD images, while the solid line shows the prediction using Eq. (9). The figure indicates that the symbolic lines were always below the corresponding solid line for the three GDLs with continuous discharge. This suggests that the droplets visualized by CCD images are always smaller than the predictions. This is because the predicted droplet radius from the fitting curve is the theoretical size of the droplet after breakthrough, but the droplet radii measured from the CCD images are "the actual droplet size on the upper surface of GDL sample." The difference between the prediction from the discharge cure and the actual data from the video image accounts for the water filling some pores in the GDL. This may then be applied for the evaluation of water saturation in the GDLs.

Moreover, for each GDL sample, both the prediction and video data of the droplet radius presented the same growing trend during the droplet growing process; they indicated that the liquid water

Fig. 11. Discharge rate comparison at 0.02 mL min^{-1} of (a) carbon paper and carbon cloth and (b) carbon cloth/MPL (LT1200W) and carbon cloth/MPL-D (HT2500W). (BT) denotes the breakthrough time.

presented the lowest discharge rate at 0.19 mL min^{-1}. A higher decay constant suggests a shorter time needed to dismiss water to the steady condition. The time from the transient to steady-state water flow rate was around 5 s for carbon cloth, about 70 s for
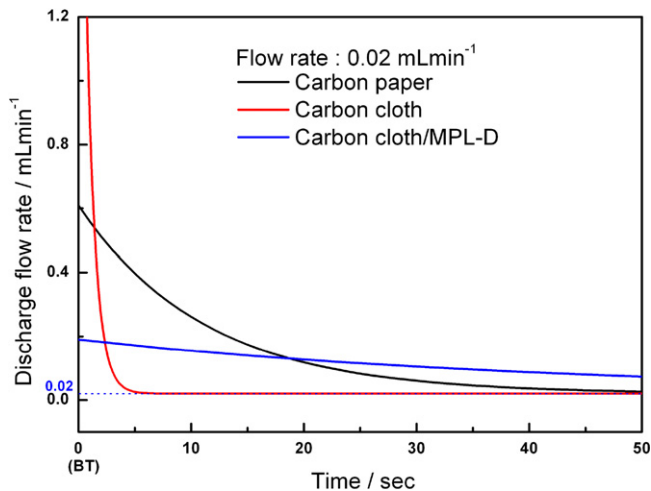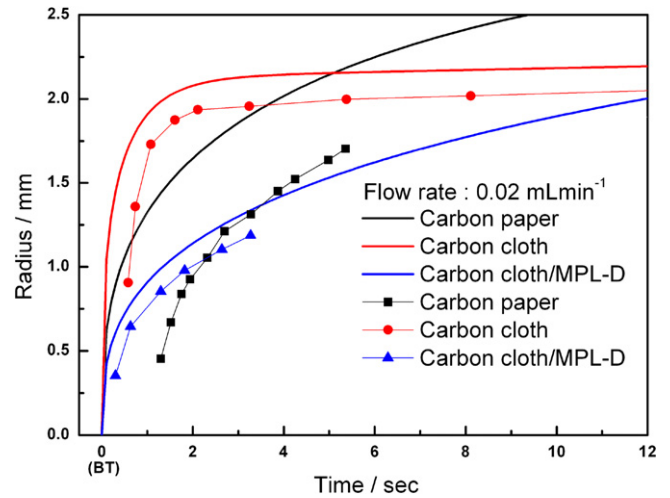

Fig. 12. Fitting curve of the discharge flow rates of GDLs after the breakthrough time.

Table 3
Liquid water saturation after breakthrough for GDLs.

GDL samples	Carbon paper	Carbon cloth	Carbon cloth/MPL	Carbon cloth/MPL-D
S_w (%)	15.3–21.2	6.5–12.8	–	2.2–2.7

trapped in the pores remains even as the injected water passes through the GDL. With the assumption that the residual liquid saturation in GDL is zero before each experiment begins, the water saturation may be evaluated by the following equation:

$$S_w = \frac{V_w}{V_p} = \frac{4/3\pi(R_{d,th}^3 - R_{d,i}^3)}{A\varepsilon d} \qquad (10)$$

where V_w is the volume of water inside the GDL sample, V_p is the GDL pore volume, $R_{d,th}$ is the droplet radius predicted from the differential pressure data, $R_{d,i}$ is the droplet radius measured by CCD images, A is the total cross-sectional area, and ε and d are the porosity and thickness of the GDL under consideration.

Table 3 shows the values of water saturation in different GDL samples using Eq. (10) after several trials. Among the three GDLs, the carbon cloth with double-sided MPL had the smallest water saturation inside. Only around 2.5% of the volume of the pores was occupied by liquid water during the percolation process. This indicates that the GDL with MPL may help reduce the water saturation, which is consistent with the results reported by Lu et al. [37] and Gostick et al. [31]. On the other hand, for the GDL samples without MPL, the carbon paper with irregular fibers demonstrated a significant larger water saturation value than the carbon cloth with regular fibers. This suggests that when the pore size distribution in the carbon paper is more uniform in both the in-plane and through-plane direction, this may help retain water inside the pore.

4. Conclusions

The liquid water breakthrough experiment through GDLs with or without an MPL was performed by the simultaneous visualization of emerging water droplets and the measurement of back pressure. The water drainage ability and the average water saturation in various GDLs were explored. Consistent with the results reported in the literature, the water breakthrough in GDLs takes place at some preferential locations and continually transports water at the same spots.

The morphology of GDLs affected the liquid water discharge flow significantly. As discussed above, a regular woven GDL had better water-dismissal ability and less liquid water saturation inside than an irregular GDL. Therefore, controlled pore distribution and large pores in the through-plane direction helped dismiss excess water. However, once the breakthrough occurred, GDL with large pores showed almost no flow resistance for water flowing through. This may let the membrane dry out easily at high operating temperatures.

The water eruption transport mechanism, which may enhance water transport, was only observed in the regular woven GDL with a single-side MPL. This violent transport may be due to the great difference in pore sizes and water saturation at the MPL/GDL interface. However, such eruptive phenomenon was not observed in the GDL with a double-sided MPL.

References

[1] H. Li, Y. Tang, Z. Wang, Z. Shi, S. Wu, D. Song, J. Zhang, K. Fatih, J. Zhang, H. Wang, Z. Liu, R. Abouatallah, A. Mazza, J. Power Sources 178 (1) (2008) 103–117.
[2] U. Pasaogullari, C.Y. Wang, J. Electrochem. Soc. 151 (3) (2004) A399–A406.
[3] U. Pasaogullari, C.-Y. Wang, Electrochim. Acta 49 (25) (2004) 4359–4369.
[4] P.K. Sinha, C.-Y. Wang, Electrochim. Acta 52 (28) (2007) 7936–7945.
[5] V.P. Schulz, J. Becker, A. Wiegmann, P.P. Mukherjee, C.-Y. Wang, J. Electrochem. Soc. 154 (4) (2007) B419–B426.
[6] X. Wang, T. Van Nguyen, J. Electrochem. Soc. 155 (11) (2008) B1085–B1092.
[7] R. Satija, D.L. Jacobson, M. Arif, S.A. Werner, J. Power Sources 129 (2) (2004) 238–245.
[8] N. Pekula, K. Heller, P.A. Chuang, A. Turhan, M.M. Mench, J.S. Brenizer, K. Ünlü, Nucl. Instrum. Methods Phys. Res. Sect. A 542 (1–3) (2005) 134–141.
[9] S. Kim, M.M. Mench, J. Electrochem. Soc. 156 (3) (2009) B353–B362.
[10] A. Turhan, K. Heller, J.S. Brenizer, M.M. Mench, J. Power Sources 160 (2) (2006) 1195–1203.
[11] I. Manke, C. Hartnig, M. Grunerbel, W. Lehnert, N. Kardjilov, A. Haibel, A. Hilger, J. Banhart, H. Riesemeier, Appl. Phys. Lett. 90 (17) (2007) 174105, 3 pp.
[12] C. Hartnig, I. Manke, R. Kuhn, N. Kardjilov, J. Banhart, W. Lehnert, Appl. Phys. Lett. 92 (13) (2008) 134106, 3 pp.
[13] C. Hartnig, I. Manke, R. Kuhn, S. Kleinau, J. Goebbels, J. Banhart, J. Power Sources 188 (2) (2009) 468–474.
[14] K. Tüber, D. Pócza, C. Hebling, J. Power Sources 124 (2) (2003) 403–414.
[15] A. Hakenjos, H. Muenter, U. Wittstadt, C. Hebling, J. Power Sources 131 (1–2) (2004) 213–216.
[16] X.G. Yang, F.Y. Zhang, A.L. Lubawy, C.Y. Wang, Electrochem. Solid-State Lett. 7 (11) (2004) A408–A411.
[17] F.Y. Zhang, X.G. Yang, C.Y. Wang, J. Electrochem. Soc. 153 (2) (2006) A225–A232.
[18] T. Ous, C. Arcoumanis, J. Power Sources 173 (1) (2007) 137–148.
[19] D. Spernjak, A.K. Prasad, S.G. Advani, J. Power Sources 170 (2) (2007) 334–344.
[20] I.S. Hussaini, C.-Y. Wang, J. Power Sources 187 (2) (2009) 444–451.
[21] A. Bazylak, Int. J. Hydrogen Energy 34 (9) (2009) 3845–3857.
[22] M.F. Mathias, J. Roth, J. Fleming, W. Lehnert, in: W. Vielstich, A. Lamm, H. Gasteiger (Eds.), Handbook of Fuel Cells: Fundamentals, Technology and Applications, John Wiley & Sons, Ltd., New York, 2003, pp. 517–537.
[23] J.H. Nam, M. Kaviany, Int. J. Heat Mass Transfer 46 (24) (2003) 4595–4611.
[24] S. Litster, D. Sinton, N. Djilali, J. Power Sources 154 (1) (2006) 95–105.
[25] A. Bazylak, D. Sinton, N. Djilali, J. Power Sources 176 (1) (2008) 240–246.
[26] A. Bazylak, J. Heinrich, N. Djilali, D. Sinton, J. Power Sources 185 (2) (2008) 1147–1153.
[27] B. Gao, T.S. Steenhuis, Y. Zevi, J.Y. Parlange, R.N. Carter, T.A. Trabold, J. Power Sources 190 (2) (2009) 493–498.
[28] E.F. Medici, J.S. Allen, J. Power Sources 191 (2) (2009) 417–427.
[29] J. Benziger, J. Nehlsen, D. Blackwell, T. Brennan, J. Itescu, J. Membr. Sci. 261 (1–2) (2005) 98–106.
[30] E. Kimball, T. Whitaker, Y.G. Kevrekidis, J.B. Benziger, AIChE J. 54 (5) (2008) 1313–1332.
[31] J.T. Gostick, M.A. Ioannidis, M.W. Fowler, M.D. Pritzker, Electrochem. Commun. 11 (3) (2009) 576–579.
[32] J.T. Gostick, M.A. Ioannidis, M.W. Fowler, M.D. Pritzker, J. Power Sources 194 (1) (2009) 433–444.
[33] J.T. Gostick, M.A. Ioannidis, M.W. Fowler, M.D. Pritzker, Electrochem. Commun. 10 (10) (2008) 1520–1523.
[34] J.D. Fairweather, P. Cheung, D.T. Schwartz, J. Power Sources 195 (3) (2010) 787–793.
[35] J.D. Fairweather, P. Cheung, J. St-Pierre, D.T. Schwartz, Electrochem. Commun. 9 (9) (2007) 2340–2345.
[36] Y.-I. Chou, Z.-Y. Siao, Y.-F. Chen, L.-Y. Sung, W.-M. Yang, C.-C. Wang, J. Power Sources 195 (2) (2010) 536–540.
[37] Z. Lu, M.M. Daino, C. Rath, S.G. Kandlikar, Int. J. Hydrogen Energy 35 (9) (2010) 4222–4233.
[38] M.M. Mench, C.Y. Wang, J. Electrochem. Soc. 150 (1) (2003) A79–A85.
[39] W. Dai, H. Wang, X.-Z. Yuan, J.J. Martin, D. Yang, J. Qiao, J. Ma, Int. J. Hydrogen Energy 34 (23) (2009) 9461–9478.
[40] K.-J. Lee, J.-H. Nam, C.-J. Kim, Electrochim. Acta 54 (4) (2009) 1166–1176.